Afterglow emission in the context of an 'one-zone' radiation-acceleration model

M. Petropoulou[1], A. Mastichiadis[1] and T. Piran[2]

1: National and Kapodistrian University of Athens, Department of Physics, GREECE
2: Racah Institute of Physics, The Hebrew University, Jerusalem, ISRAEL

Abstract

In the present work, we focus on the interplay between stochastic acceleration of charged particles and radiation processes in a region of turbulent magnetized plasma, setting the framework for an "one-zone" radiation-acceleration model for GRB afterglows. Specifically, we assume that the particle distribution is isotropic in space and treat in detail the particle propagation in momentum-space. The electron distribution is modified by the acceleration, radiation (synchrotron/SSC) and escape processes. The magnetic field as well as the particle injection rate are functions of time as measured in the co-moving frame of the blast wave. We numerically solve the time-dependent Fokker-Planck equation and present characteristic examples for the obtained particle and photon spectra.

Introduction

Afterglow emission originates from an external shock that is formed by a relativistic blast wave propagating in the surrounding medium (e.g. *Meszaros & Rees 1997*). The non-thermal character of the afterglow emission suggests the formation of a high-energy particle population through an acceleration mechanism. Thus, a self-consistent model for the afterglow emission should combine the acceleration and radiation processes of particles, as the physics of the problem implies.

Particle acceleration at (ultra)relativistic shocks has been studied in the test particle approximation both analytically (*Kirk et al. 2000; Waxman & Keshet 2005*) and numerically using Monte Carlo simulations (*Bednarz & Ostrowski 1998; Achterberg et al. 2001*). The resulting particle spectra can be modelled as power-laws of exponent p~2.3-2.4. More recently PIC simulations (*Spitkovski 2008*) that take into account the back-reaction of accelerated particles onto the shock structure show that the particle distribution consists robustly of two components: (i) a relativistic Maxwellian and (ii) a power-law tail. Based on the results of particle acceleration theory and simulations, the majority of works for *radiative signatures* from GRB afterglows uses an already accelerated power-law particle distribution. A first effort to combine stochastic acceleration and adiabatic losses for particles in a GRB blast wave shell using the kinetic equation approach was made by *Dermer & Humi (2001)*.

Aims of the present work are:

- The combination of stochastic acceleration and radiation processes into a time-dependent 'one-zone' model specified on the afterglow emission.
- The study of the parameter-space based on the morphologies of the obtained electron and photon spectra.

The model

We consider an adiabatic blast wave with initial energy E_0 and Lorentz factor Γ_0 that propagates into an external medium of constant number density n_0. We assume a mono-energetic electron injection at $\gamma_{inj} \sim \Gamma(r)$, in the blast wave shell of co-moving width $\Delta' = r/\Gamma(r)$, containing a magnetic field of strength $B = (32 \pi n_0 m_p \varepsilon_B c^2)^{1/2} \Gamma(r)$. On the one hand, injected particles are being stochastically accelerated through resonant scattering with turbulent MHD waves, while on the other hand they suffer energy losses through synchrotron and SSC emission. For the turbulence we assume a power-spectrum $w(k)dk \sim k^q dk$, with the exponent lying typically in the range 1-2. Escape of particles from the acceleration/radiation region is also taken into account.

Simplifying assumptions

1. Test-particle approximation.

2. The particle distribution in the shell is isotropic. Thus, we can ignore the details of particle transport in space and focus on their propagation in momentum-space.

3. An energy dependent escape term treats approximately the problem of spatial confinement of the particles in the acceleration region.

4. The distribution of emitted photons is not treated through a separate equation. The emitted synchrotron spectrum at each co-moving time t' is obtained from the convolution of the synchrotron emissivity function and the electron distribution.

5. Synchrotron radiation fills instantaneously the shell. Thus, SSC spectra at a time t' are obtained from the convolution of the synchrotron photon and electron distributions at the same time. No photon travel effects are taken into account for this calculation.

Fokker-Planck equation

$$\frac{\partial n}{\partial t'} + \frac{n}{t_{esc}(\gamma, t')} = \frac{\partial}{\partial \gamma}\left[-\left(\dot{\gamma}_{loss}(\gamma, t') + \frac{D(\gamma, t')}{\gamma}\right)n + D(\gamma, t')\frac{\partial n}{\partial \gamma}\right] + Q(\gamma, t')$$

Definition of functions appearing in eq. Fokker-Planck

Escape timescale $\qquad t_{esc}(\gamma, t') = t_{dyn}(t')\gamma^{q-2}$

Acceleration timescale $\qquad t_{acc}(\gamma, t') = \tau_{acc}(t')\gamma^{2-q}$

Diffusion coefficient $\qquad D(\gamma, t') = \frac{\gamma^2}{2t_{acc}(\gamma, t')}$

Energy loss rate $\qquad \dot{\gamma}_{loss}(\gamma, t') = \frac{-4\sigma_T}{3m_e c^2}\left[u_B(t') + u_{syn}(\gamma, t')\right]\gamma^2$

Synch. photon energy density $\qquad u_{syn}(\gamma, t') = \frac{4\pi}{c}\int I'_{syn}(\nu', t')d\nu'$

Injection rate $\qquad Q(\gamma, t') = \xi c \Gamma^2(r)n_0 r^{-1}\delta[\gamma - \Gamma(r)]$

Here ξ is the fraction of the kinetic energy that is used for acceleration of particles and $t_{dyn} = r/c\Gamma(r)$ is the dynamical scale of the problem.

Results

We present results obtained from the numerical solution of the Fokker-Planck equation for three example cases, where we assumed $E_0 = 10^{53}$ erg/s, $\Gamma_0 = 100$, $n_0 = 1$ par/cm³. A redshift z=0.1 was used throughout the present work.

Case 1: t_{acc} = constant and $t_{esc} = t_{esc}$ (r)

Here we examine the "hard sphere" approximation, i.e. q=2.

We present two examples with: (a) "fast" acceleration and strong magnetic field and (b) "slow" acceleration and weak magnetic field. The acceleration is characterized "slow" or "fast" with respect to the deceleration dynamical timescale, i.e. $t_{dyn}(R_d) \approx 8 \times 10^4 s$

The parameters used for the examples are given below:

(a) t_{acc} =10³ s, ε_B=0.1, ξ=0.1	(b) t_{acc} =10⁵ s, ε_B=0.001, ξ=0.1

PARTICLE DISTRIBUTIONS
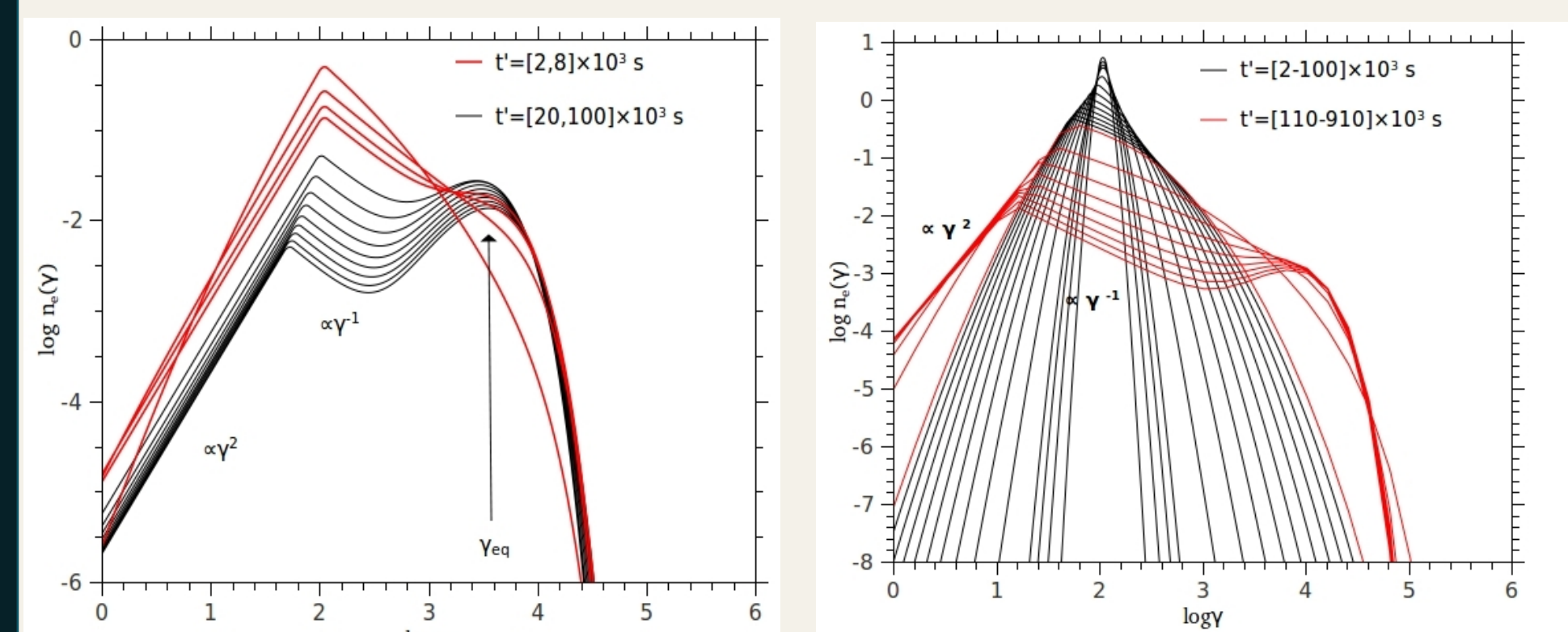
FIGURE 1: Snapshots of the evolving electron distribution at early (red lines) and late (black lines) times with respect to t_{acc}. The quadratic dependence at low-energies and the exponential cutoff at high-energies are characteristics of the second order acceleration process.

FIGURE 2: Symbols same as in Fig.1. Because of the slower acceleration, the distribution does not reach the maximum energy at t'=10⁵ s, in contrast to the case shown in Fig.1. Moreover, the magnetic field is weaker and the synchrotron losses truncate the distribution at a higher Lorentz factor than in Fig.1.

Comments:
- In Fig.2 the particle distribution accelerates slowly because of the large acceleration timescale. For this reason the distribution does not extend up to the maximum energy at t'=10⁵ s. This explains also the density of the snapshots in contrast to that of Fig.1.
- Because of the weaker magnetic field, the acceleration saturates due to synchrotron losses at a higher Lorentz factor than in Fig.1.
- Although the distribution does not reach a steady state, at late times it evolves in both cases in a self-similar way.

OBSERVED PHOTON SPECTRA
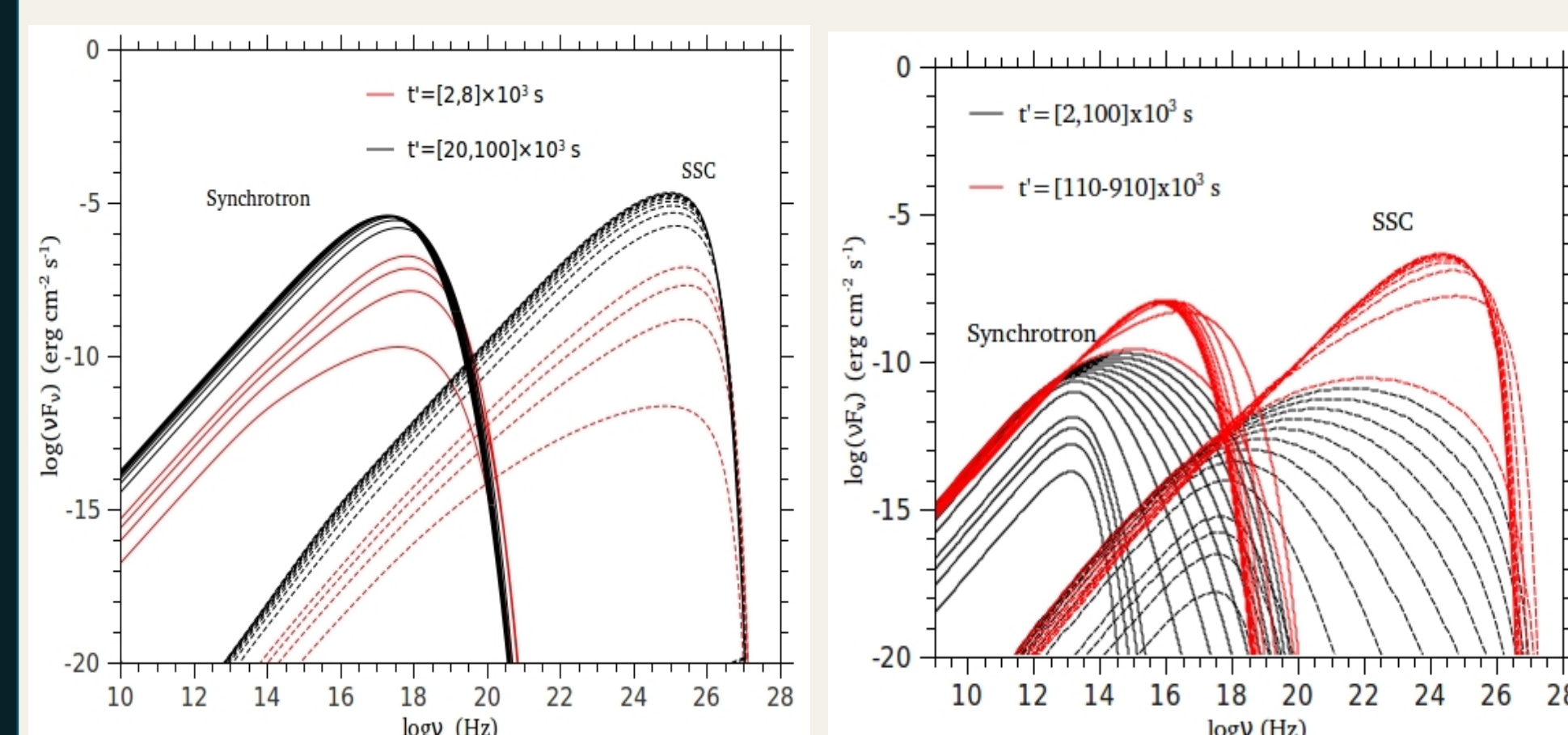
FIGURE 3: Time evolution of the observed synchrotron (solid lines) and SSC (dashed lines) spectra. The relative ratio of the synchrotron/SSC peak changes during the evolution. The peak position of the synchrotron spectrum remains constant (black lines).

FIGURE 4: Symbols same as in Fig.3.

Comments:
- In both examples the acceleration is saturated due to synchrotron losses. The observed peak synchrotron frequency is constant during the deceleration of the blast wave , i.e. $\gamma_{eq} \propto B^{-1} \Rightarrow \nu^{obs}_{s,max} \propto \Gamma B\gamma^2_{eq} = const$
- The relative ratio of the synchrotron/SSC peak luminosity varies with time starting with values less than unity. The fact that particle escape becomes less efficient at late times combined with the decrease of magnetic field strength leads to an SSC dominance of the spectra at late times.

Case 2: $t_{acc} = t_{acc}$ (γ) and $t_{esc} = t_{esc}$ (γ,r)

Here we focus on a case with turbulent exponent q=1/2. The explicit expressions for the acceleration and escape timescale used are:

$$t_{acc} = 10^3 \left(\frac{\gamma}{10^5}\right)^{3/2} s \qquad \text{and} \qquad t_{esc} = 10^{9/2}t_{dyn}(r)\left(\frac{\gamma}{10^5}\right)^{-3/2} s$$

Other parameters used: $\varepsilon_B = 10^{-3}$, $\xi = 2 \times 10^{-3}$

In this case a time-decreasing observed synchrotron peak frequency can be obtained (see the last two snapshots of Fig.6). This is suggested by the following relations:

★ If the acceleration process is saturated due to particle escape:
$$\gamma_{eq} \propto t^{1/3}_{dyn} \Rightarrow \nu^{obs}_{s,max} \propto \Gamma B\gamma^2_{eq} \propto r^{-4/3}$$

★ If the acceleration process is saturated due to synchrotron losses:
$$\gamma_{eq} \propto B^{-2/5} \Rightarrow \nu^{obs}_{s,max} \propto \Gamma B\gamma^2_{eq} \propto r^{-9/5}$$
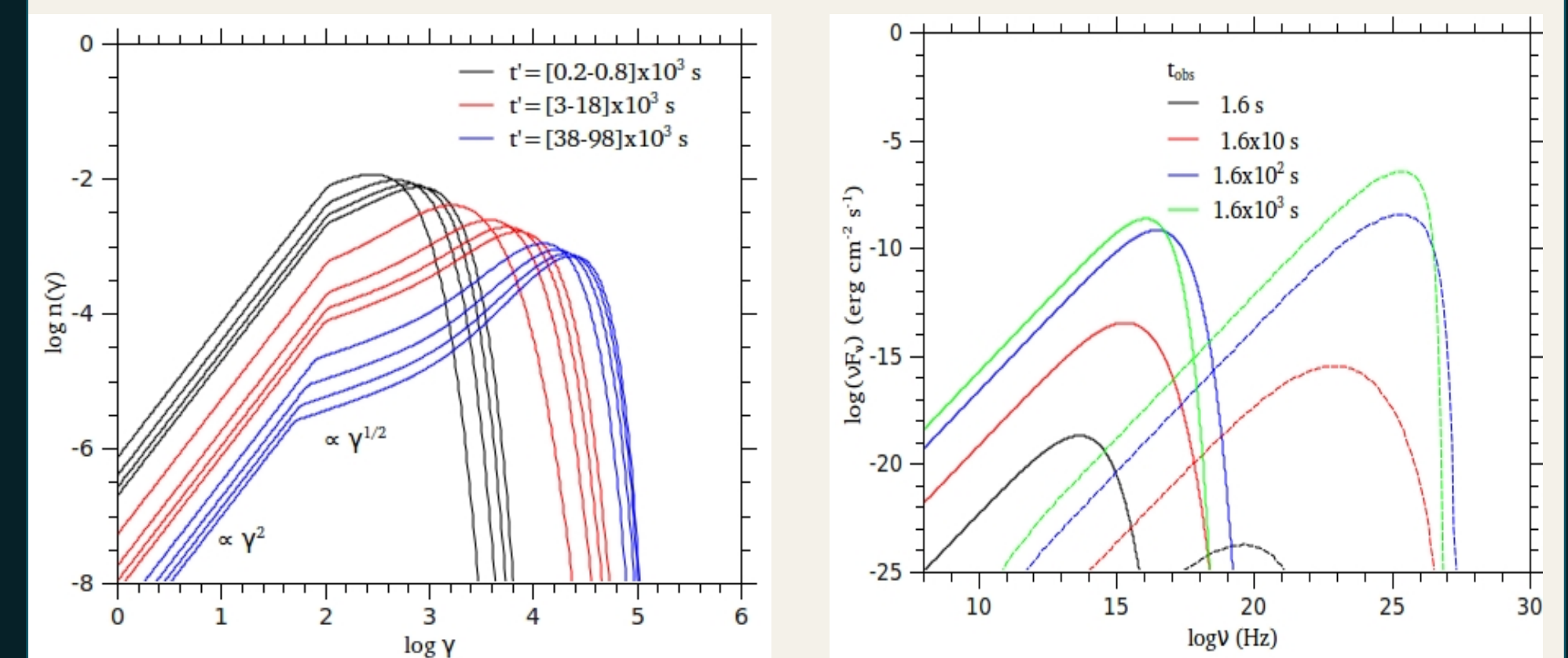
FIGURE 5: Snapshots of the electron distribution. The slope 0.5 of the particle distribution is typical of the specific turbulent spectrum exponent. It is obtained for that range of Lorentz factors, for which the acceleration process is the fastest among the escape and synchrotron losses.

FIGURE 6: Time evolution of the observed photon spectra. The peak frequencies of the synchrotron and SSC components decrease with time during the deceleration of the blast wave (blue and green lines).

Case 3: $t_{acc} = t_{acc}$ (γ,r) and $t_{esc} = t_{esc}$ (γ,r)

In the previous cases we have treated the normalization of t_{acc} as a free parameter. Here we adopt an expression for the diffusion coefficient (e.g. *Melrose 1968; Schlickeiser 1989*) corresponding to $t_{acc}(\gamma, t') = \tau_{acc}(t')\gamma^{2-q}$

where the normalization is $\tau_{acc} = (2\pi)^{q+1}n_0 m_p c^2\left(\frac{m_e c^2}{e}\right)^{2-q}\zeta^{-1}B^{q-4}(t')t^{q-1}_{dyn}(t')$

and $\zeta = \frac{\int W(k)dk}{B^2/8\pi}$ is the ratio of the turbulent energy density to that of the large-scale magnetic field.

This choise reduces the number of free parameters, which for this example are: $q=1, \varepsilon_B = 1.2 \times 10^{-5}, \zeta = 10^{-5}, \xi = 0.1$
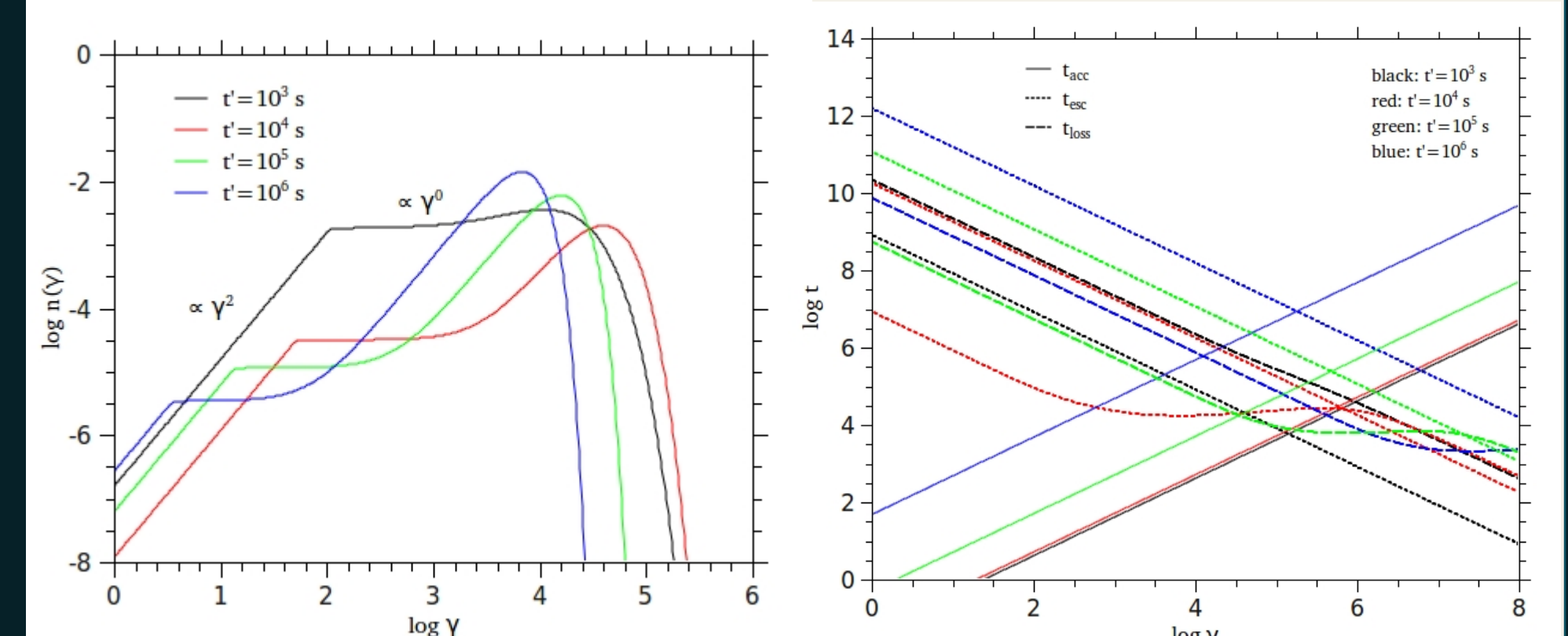
FIGURE 7: Evolution of the electron distribution. At early stages (t'<10⁴ s) acceleration and escape processes determine the shape of the distribution. Energy losses become important at later times (t>10⁴ s) and escape of particles is inefficient. Thus, particles tend to pile up at the equilibrium energy, forming a bump.

FIGURE 8: Characteristic timescales (lines of different type) as a function of the Lorentz factor γ. Different colours denote different times. In this case the time evolution of the system is not trivial.
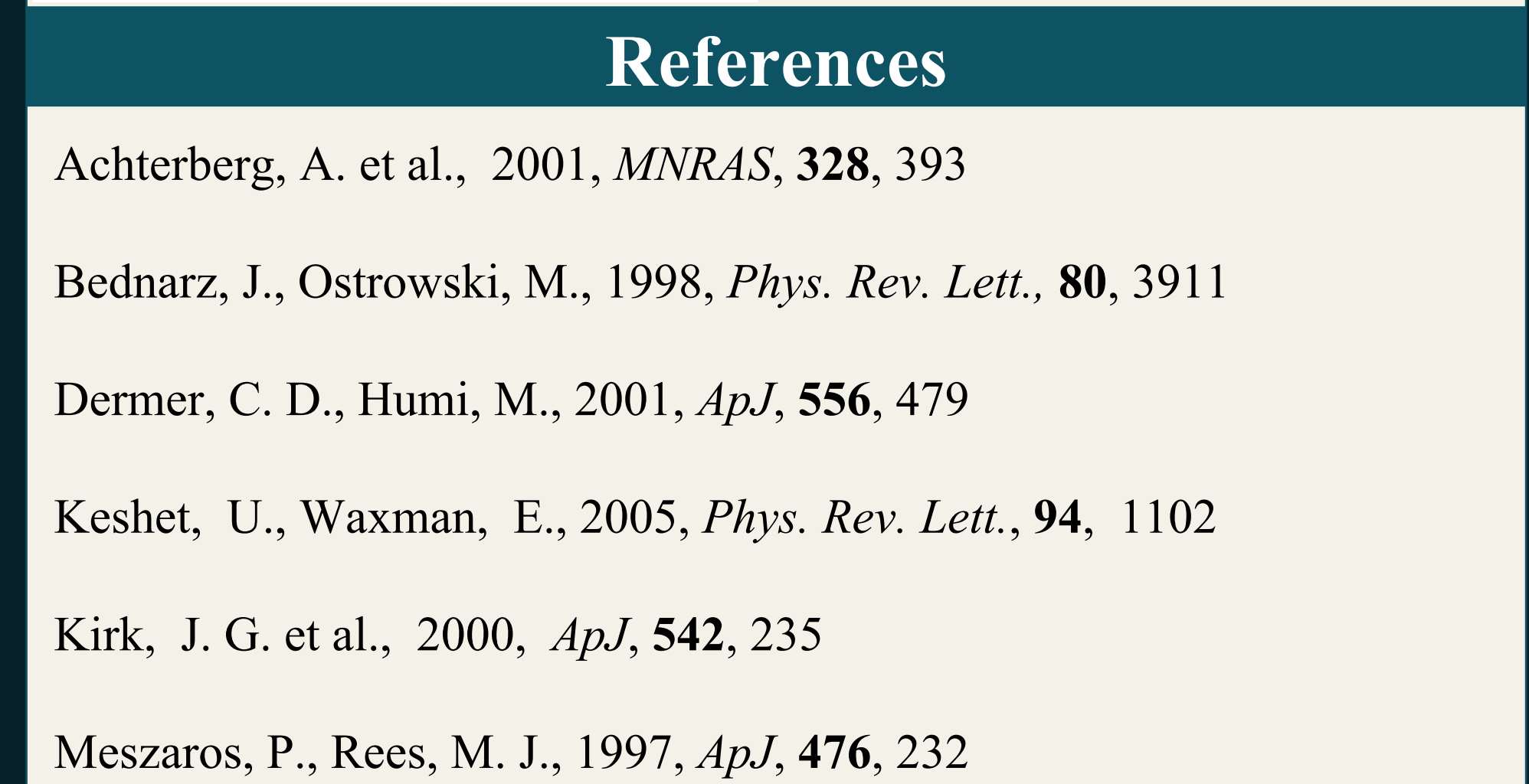
FIGURE 9: Same as Fig.7 but replotted for the quantity γ² n, which is a measure of the particle energy content. Although the number of particles accumulated at the cutoff of the distribution increases with time (see Fig.7), the energy content starts decreasing from t' > 10⁴ s.

References

Achterberg, A. et al., 2001, *MNRAS*, **328**, 393

Bednarz, J., Ostrowski, M., 1998, *Phys. Rev. Lett.,* **80**, 3911

Dermer, C. D., Humi, M., 2001, *ApJ,* **556**, 479

Keshet, U., Waxman, E., 2005, *Phys. Rev. Lett.,* **94**, 1102

Kirk, J. G. et al., 2000, *ApJ,* **542**, 235

Meszaros, P., Rees, M. J., 1997, *ApJ,* **476**, 232

Spitkovsky, A. 2008b, *ApJ,* **682**, L5

Acknowledgments